ISSN 1840-4855
e-ISSN 2233-0046

Original scientific article
http://dx.doi.org/10.70102/afts.2026.1835.232

INVESTIGATION INTO THE OPTIMAL THERMAL EFFICIENCY OF A POROUS MEDIUM INSIDE A DUCT CONTAINING GLASS BEADS

Mohammed Z. Hameed[1*], Musa Weis Mustafa[2]

[1]Department of Technical Thermal Engineering, Technical Engineering College of Kirkuk, Northern Technical University, Iraq. e-mail: mohammed.zaidan24gs@ntu.edu.iq, orcid: https://orcid.org/0009-0003-6122-207X*
[2]Department of Technical Thermal Engineering, Technical Engineering College of Kirkuk, Northern Technical University, Iraq. e-mail: musa.weis@ntu.edu.iq, orcid: https://orcid.org/0000-0002-2224-9224

Received: January 03, 2026; Revised: February 18, 2026; Accepted: April 08, 2026; Published: May 29, 2026

SUMMARY

In the current experimental study, a rectangular channel packed with a porous medium is used to study the thermo-hydraulic performance of a forced convection air heater. In addition to heat transfer enhancement, various experimental setups (Works 1 to 4) have been used to investigate the combined effects of the disruption of the thermal boundary layers and flow resistances for different values of the Reynolds number, which was achieved through the geometric configuration of a horizontal cylindrical heater placed in the porous medium. The results reveal that, in contrast to the baseline case of an empty channel, adding the porous medium has an enormously enhanced ability to heat up the Air. While having an optimal improvement of 358.05% for lower flow speeds in increasing the maximal Nusselt number, the optimal configuration (Work 4) performed best in purely thermal efficiency considerations. However, despite such performance enhancement, there is also an inevitable increase in the static pressure drop, which was also found to follow a non-linear for cheider model. To evaluate the practical applicability of such modifications in relation to their performance improvement in an effective manner, the Performance Evaluation Criteria (PEC) index was also considered in this study.

Key words: *porous media; forced convection, heat transfer enhancement, nusselt number, geometric optimization, wall temperature reduction.*

INTRODUCTION

Porous media convective heat transfer has been of great interest in the recent past because of its usage across a broad range of industries such as geothermal systems, electronic cooling, chemical reactors, and solar air heaters [1]. The main problem with these thermal systems is that they are intrinsically resistant to heat flow due to the formation of thermal boundary layers. It is important to make these systems more efficient in order to minimize energy usage and to decrease the physical dimensions of the thermal exchange apparatus [2].

Significance of the Study: The conventional heat exchangers are prone to low heat transfer coefficients with Air as the working fluid. It has been found that altering the internal geometry or even inserting may cause a major disturbance of these boundary layers [3]. Although incorporating porous media like glass beads is an established technique to increase the turbulence and mixing [4], little consideration is usually given to how the geometric configuration of the source of heat is arranged in that media. It is also important to know the exact location of the heater in the porous matrix to maximize thermal performance [5] and also ensure that the hydraulic penalty (pressure drop) remains at manageable levels by industrial fans and blowers [6].

Contribution of the Work: Previous studies have explored various aspects of porous media, ranging from the impact of pore density to the thermal conductivity of the solid matrix [7]. Some researchers have focused on the mathematical modeling of fluid flow in packed beds [8], while others have examined the effects of different shapes of cylinders on heat transfer [9]. However, there remains a gap in the literature regarding the optimization of a horizontal cylindrical heater's position, specifically within a confined rectangular duct filled with spherical glass beads.

This study contributes to the field by providing a comprehensive experimental analysis of four distinct geometric configurations (Works 1–4). The unique contribution of this research is the identification of an optimal thermal zone within the porous matrix that maximizes the Nusselt number, achieving an improvement of up to 358.05% compared to empty channels. Furthermore, the study provides empirical data correlating the thermal gains with the non-linear pressure drop according to the Forchheimer model, offering a practical design benchmark for thermo-hydraulic engineering [18] [20].

The rest of this manuscript will be structured in the following manner: Section 2 will contain a literature review. Section 3 describes the research experimental layout, which includes the wind tunnel design, characteristics of the glass beads, and geometries of the four experimental configurations, and gives the mathematical model and equations of thermodynamics and hydraulic analysis. Section 4 is the discussion on the results, where the heat transfer rates, wall temperatures, and pressure drop in each of the cases are compared. Finally, Section 5 summarizes the study by making important findings and future suggestions on how to make thermal systems more efficient.

LITERATURE REVIEW

In an attempt to gain an understanding of the fundamental percolation, the first experimental works were focused on natural and mixed convection. Internal temperature stratification and the depth of flow penetration depend on the opening ratio and boundary conditions, based on the experiments done on the partially-opened cavities containing porous medium [10]. In the same manner, the experimental works regarding the “partial open side effect” of porous cavities indicated that the level of natural convection is remarkably affected by the structure of the inlet and outlet ports [13]. Going back to the experiment done on duct flow, the direction of the channels becomes highly important. The role of convective heat transfer, assisted by buoyancy, is diminished due to an increase in flow resistance, based on the experimental works done on the convection of the vertical porous tube [11][12]. Although the porous medium tends to equalize the temperatures, the pressure difference penetrating the bed is the determining constraint during mixed convection, based on the experimental works done on the horizontal and inclined circular tubes [16].

Various insertion strategies have been considered to minimize hydraulic drag in forced convection conditions, which is also addressed here with respect to air heating. Experiments conducted on square channels compared the 'simple' and 'partly inserted' porous medium and showed that partial insertion is preferable to complete insertion because it allows bypass flow and thus reduces the overall pressure loss [14]. Research on units utilizing latent heat storage, which showed that the optimization of volume percentage of the porous medium proved more efficient than the mere increase in volume percentage of the porous medium, further supports this theory [17]. Disruption of the porous medium helps in the promotion of flow and turbulence and increases the efficiency with lower pumping power requirements compared to solid porous blocks, as shown by various experiments on single-phase flow through channels with staggered porous blocks [19] (Table 1).

Table 1. Summary of key literature regarding heat transfer in porous media

Ref.	Geometry / Setup	Porous Media / Fluid	Flow Regime	Key Findings / Engineering Outcome
[10]	Concentric vertical annular tube	Porous media / Water	Forced Convection	Porous media improves heat transfer; optimal permeability limits pressure drop penalties.
[12]	Cylinder embedded in porous media	Porous bed / Air	Forced Convection	Nu is correlated with Re and Darcy number; boundary layer thinning is observed.
[14]	Square channel (Plain vs. Inserted)	Porous blocks / Air	Forced Convection	Partial insertion offers better thermal-hydraulic performance than full filling (lower ΔP).
[15]	Vertical channel	Porous glass balls (varying diameters) / Air	Forced Convection	Smaller beads enhance heat transfer but increase pressure drop; an optimal size balances performance.
[16]	Channel with different cross-sections	Glass spheres / Air	Turbulent Flow	Confinement ratio (Channel $D_h/$ Particle $\boldsymbol{d_p}$) governs wall channeling effects.
[18]	PV module with integrated cooling channel	Porous media layer / Water	Forced Convection	Water-cooled porous media lowers PV temperature, boosts electrical efficiency, and reduces pressure drop with higher permeability.
[19]	Heated triangular cylinder	Porous media / Air	Forced Convection	Sharp corners of the heater induce localized vortex shedding within the porous bed.
Current Study	Rectangular Channel with Cylinder	Spherical Beads / Air	Forced Convection	Investigates optimal heater positioning (H/V) considering both ΔP and Air Heating Efficiency.

EXPERIMENTAL SETUP AND METHODOLOGY

Experimental Facility and Instrumentation

A specifically designed open-loop wind tunnel, aimed at mimicking the process of forced convection air heating under controlled hydrodynamic conditions, was employed within the experiment. A picture of the actual experimental setup is depicted in figure 1, which also indicates the actual setup of the data acquisition system, power control unit, and air system implemented within the experiment. Figure 2 is a comprehensive schematic representation of the overall air flow circuit, which clearly indicates the functional order of the various components.

The data was recorded as experimental data through [software, e.g., LabVIEW or Excel Data Logger]. The Forchheimer pressure drop model was statistically analyzed and fitted with OriginPro 2024 (or MATLAB), and the non-linear least-squares regression algorithm was used to maximize the coefficient of determination ($R^2 > 0.98$).

The main experimental parameters to be applied in the study are: the temperature of the inlet air was 298 0.5 K because the thermal conditions of the boundaries were to be controlled. The packed bed will be composed of glass beads, which have a uniform diameter of 15 mm and a porosity of 0.39, which is a fraction of void in the duct. The power input to the heater is changed to 50-200 W to investigate the behavior of heat transfer at varying thermal loads. The duct geometry has an aspect ratio (W/H) of 2.5, and this aspect ratio is constant in all experiments in order to be geometrically consistent.

Figure 1. Photographic view of the experimental test rig and instrumentation

A high-capacity centrifugal blower (0.55 kW) sucks in atmospheric Air through a bell-mouth inlet to produce flow. A manual gate valve is provided immediately downstream of the blower to control the flow rate. Air flow then passes through a calming section with fine wire meshes and a honeycomb straightener to damp out swirl and turbulence. This ensures that Air enters the test section with a uniform velocity profile. From the schematics, it is evident that a calibrated orifice plate flow meter with a U-tube manometer is employed to measure air mass flow rate ($\dot{m}_{\text{air}}$) with high accuracy. Flow rate is measured using the standard discharge equation based on the orifice pressure difference ($\Delta h_{\text{ori fice}}$), as shown in equation (1).

$$\dot{m}_{\text{air}} = C_d A_o \sqrt{2\rho_{\text{air}}\, g \Delta h_{\text{orifice}}} \rightarrow \qquad (1)$$

where g is the value of gravity acceleration, A_0 is the cross-sectional area of the orifice, ρ_{air} is the density of Air, and C_d is the discharge coefficient of the orifice plates.

The test section has a considerable amount of equipment available to record hydraulic and thermal data. A high-accuracy differential pressure gauge is connected to the pressure taps located at the inlet and outflow of the test channel to record the static pressure drop (ΔP) through the porous material. Figure 2 illustrates different pressure measuring equipment used in this study, such as the differential-pressure gauge for the channel pressure drop and the U-tube manometer for the flow rate.

Calibrated T-type (Copper-Constantan) thermocouples are employed for temperature measurements. The bulk temperature of the incoming cold Air (T_{in}) is measured using a matrix of thermocouples at the channel's intake, and the heated air (T_{out}) temperature is detected using a matrix of thermocouples at the channel's outlet. An electrical resistance heating cartridge is employed to heat a copper cylinder, acting as the heating source. An AC variac transformer is utilized for regulating the heating source's electrical power supply to maintain a constant heat flux process. The measured electrical voltage (V) and current (I), supplying the heating source, enable the electrical power (Q_{in}) to be determined in equation (2).

$$Q_{in} = V \cdot I \rightarrow \qquad (2)$$

Figure 2. Instrumentation used for pressure and flow measurements (manometers)

The steady-state heat transfer rate absorbed by the Air (Q_{air}) is determined from an energy balance across the test section shown in equation (3):

$$Q_{\text{air}} = \dot{m}_{\text{air}}\, c_{p,\text{ air}} (T_{\text{out}} - T_{in}) \rightarrow \qquad (3)$$

Where $c_{p,\text{ Air}}$ is the specific heat capacity of Air at constant pressure. The average convective heat transfer coefficient (h_{avg}) and the corresponding average Nusselt number (Nu_{avg}) are then calculated based on the log mean temperature difference (LMTD) and the channel hydraulic diameter (D_h) represented in equations (4) and (5):

$$h_{avg} = \frac{Q_{air}}{A_s \cdot \Delta T_{LMTD}} \rightarrow \quad (4)$$

$$Nu_{avg} = \frac{h_{avg} D_h}{k_{air}} \rightarrow \quad (5)$$

Where A_s is the surface area of the heated tube and k_{air} is the thermal conductivity of Air. These governing equations form the basis for the data reduction process utilized throughout this study.

Test Section Geometry and Heating Element Details

The crucial area of the experimental setup is the test section, which is designed to facilitate a detailed study of forced convection heat transfer phenomena in various hydrodynamic conditions. A detailed sketch of the test section geometry is depicted in figure 3, indicating the accurate sizes as well as the position of internal components. This test section is 10 mm thick with a clear acrylic resin material (Plexiglass). Notably, the low thermal conductivity of this material ($k \approx= 0.19 \text{ W/m} \cdot \text{K}$) significantly suppresses the conductive heat loss to the surrounding Air, such that the heat transfer measurement can be attributed to the convective heat flux in the test section. This material is chosen for the test section for the following reasons: it allows for optical access for observation of the flow characteristics as well as porous media configuration. Furthermore, the test section is designed with a rectangular cross-section that is of sufficient length (L) to ensure that the test section is under fully developed flow before measuring heat transfer. Its width (W) and height (H) remain fixed.

One of the key characteristics is that it possesses a heated copper tube as its heated surface area. Copper is selected for its excellent thermal conductivity properties that reduce the conduction resistance in the direction of the circumference, ensuring that the surface temperature of the passage approaches uniformity. Additionally, the heated tube is positioned at the center for the sake of symmetry with respect to the passage walls, as depicted in the figure, such that the airflow isnot skewed. To designate the regimes of airflow through the non-circular duct, the Reynolds number is evaluated using the hydraulic diameter (D_h), which is determined using the cross-sectional area (A_c) of the rectangular channel with a wetted perimeter (P) by the relationship given below in equation (6):

$$D_h = \frac{4A_c}{P} = \frac{4(W \times H)}{2(W + H)} = \frac{2(W \times H)}{(W + H)} \rightarrow \quad (6)$$

Calibrated T-type thermocouples must be placed correctly for effective thermal analysis of the system. Some of the thermocouples are installed in the copper tube to record the surface temperature of the system with a degree of accuracy (T_{wall}).

These sensors are arranged both axially along the length of the tube and at fixed angular locations ($0°, 90°, 180°$, and $270°$) as depicted in the detailed view of figure 3. This is crucial for determining the(local) variations of heat transfer coefficients that result from the formation of wakes, boundary layers, and impingement zones. The thermocouple elements are embedded in minute grooves that are machined on the surface of the tube and polished flat to retain hydrodynamic surface integrity that could otherwise be disturbed by the presence of the heat transfer sensors. Additionally, the use of thermocouple arrays located at cross-sections upstream and downstream of the heated section allows for the measurement of air temperature at the intake section (T_{in}) and outlet sections (T_{out}), ensuring that an average representation of the thermal energy gained by the fluid is captured.

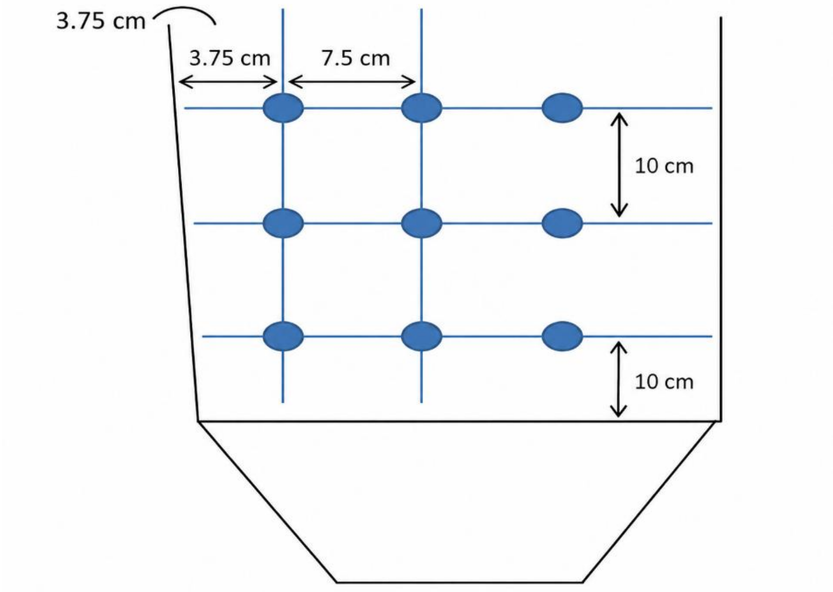

Figure 3. Schematic diagram of the test section geometry and detailed dimensions

Internal Assembly and Heat Source Arrangement

As shown in figure 3, the three-dimensional isometric drawing of the test section clearly shows the position of the heat source relative to the porous region. A heated cylinder is actually the centerpiece of this test section, which is placed coaxially in a rectangular channel. Both ends of the cylinder are fixed using thin, aerodynamic struts made of non-conductive material called Teflon. This ensures that it remains concentric with no possibility of any vibrations caused by high air speeds. These struts are thin to ensure that no wakes are formed that could hamper the heat transfer at the front end of the heating surface.

The major passive means of enhancement is by means of the densely packed porous material that encircles the core heating point. The randomly packed elements, which are spherical in shape, fill the annular region between the tube surface and the walls of the channel, as depicted in the isometric view. A support mesh fixed at the downstream boundary of the test section prevents the packed bed from being displaced by the drag forces developed by the airflow. This mesh is constructed from high-tensile stainless-steel wire with a grid aperture size carefully selected to be slightly smaller than the diameter of the packing spheres, (d_p). This is one of the design specifications that creates little resistance to the airflow while ensuring that the structural integrity of the porous matrix is established. This is evident from the clarity of figure 4 on how this porous matrix is designed to ensure that the porosity (ϕ) of the air phase remains consistent throughout the experiment.

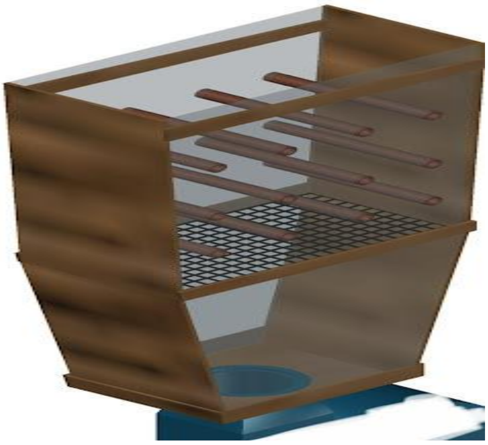

Figure 4. 3D isometric view of the test section showing the internal tube arrangement and support mesh

Due to its influence on hydrodynamics and the availability of the surface area, the structure of the porous material is of vital importance. A key characteristic that emerges is the ratio of the volume that is accessible for the flow (V_{void})to the total volume of the test section, (V_{total}). This is measured by the porosity or void fraction (ϕ) of the bed, which is determined through the following relationship shown in equation (7):

$$\phi = \frac{V_{\text{void}}}{V_{\text{total}}} = 1 - \frac{V_{\text{solid}}}{V_{\text{total}}} = 1 - \frac{\sum_{i=1}^{N} \frac{\pi}{6} d_p^{\beta}}{W \times H \times L} \rightarrow \qquad (7)$$

In this configuration, N denotes the number of spherical particles packed into the microchannel, which depends on the width (W), height (H), and length (L) of the microchannel. An isometric drawing is crucial to understanding geometric complexities since it allows one to understand points of contact between the particles and the heated surface. These points of contact effectively work like bridges for heat conduction since airflow is channeled through a meandering path by the minute distances between particles. While such a situation could be viewed from a 2D perspective without significant loss of clarity, it is evident that the 3D representation clearly elucidates how the desired boundary layer disruption and enhanced mixing are achieved through such forcing. It is important to note that the internal geometry is carefully optimized to be a hydrodynamic area that is intended to enhance interactions between solid and fluid phases, as opposed to purely structural considerations.

Data Reduction and Governing Equations

The dimensionless performance parameters that control the system's thermal and fluid dynamic behavior were determined from the raw data of the data acquisition system, which included temperatures, pressure differences, and electric signals. The bulk mean temperature, T_b, which is the arithmetic average of the input and outlet air temperatures, is used to determine all the thermo-physical properties of the Air, such as air density, ρ, dynamic viscosity, μ Air thermal conductivity, k, and Air specific heat, Cp, as shown in equation (8).

$$T_b = \frac{T_{\text{in}} + T_{\text{out}}}{2} \rightarrow \qquad (8)$$

Correlation between inertial and viscous forces in the channel is expressed through the Reynolds number (Re), which is the basic independent variable. This value is calculated with the help of the mean speed of air (U_{avg}) and the hydraulic diameter (D_h) of the channel in equation (9):

$$Re = \frac{\rho U_{avg} D_h}{\mu} = \frac{4\dot{m}}{\mu P_{wet}} \rightarrow \qquad (9)$$

A heat balance analysis at the point of steady state was performed, and the intention was to confirm the thermal values read from the system. The actual heat absorbed by the airflow (Q_{air}) and the electrical heat input given to the heater element (Q_{in}) were compared, and from Newton's Cooling Law, the heat transfer coefficient (h) took into account the streamwise variations of temperature, which were based on the logarithmic mean temperature difference (ΔT_{LMTD}) represented in equations (10)(11)(12):

$$Q_{\text{air}} = \dot{m} c_p (T_{\text{out}} - T_{in}) \rightarrow \qquad (10)$$

$$h = \frac{Q_{\text{air}}}{A_s (T_{\text{wall}} - T_b)} \rightarrow \qquad (11)$$

$$Nu = \frac{h D_h}{k} \rightarrow \qquad (12)$$

Here, Nu is the mean Nusselt number, T_{wall} is the mean tube surface temperature, and A_s is the peripherial surface area of the tube with heat applied.

It is important to note that the calculation of the hydraulic penalty due to the use of porous media is a major aspect in this study. The Darcy friction factor (f) was calculated using the pressure losses ΔP measured during the test section. A useful heat exchanger design requires the calculation of the above parameter, which is a measure of flow resistance. The Darcy-Weisbach equation is used to determine the value of (f) shown in equation (13):

$$f = \frac{\Delta P \cdot D_h}{2L\rho {U_{avg}}^2} \rightarrow \tag{13}$$

The relative volume of voids to total volume is indirectly given by the porosity of a packed bed (ϕ), which is essentially dependent on both permeability and pressure drop. The essential dimensionless quantities, utilized in this study, are given below in table 2, along with their physical significance.

Table 2. Definition of dimensionless groups used in the data reduction

Dimensionless Group	Symbol	Definition	Physical Significance
Reynolds Number	Re	$\frac{\rho U D_{\mathrm{L}}}{\mu}$	Ratio of inertial forces to viscous forces.
Nusselt Number	Nu	$\frac{hD_h}{k}$	Ratio of convective to conductive heat transfer.
Prandtl Number	Pr	$\frac{q\mu}{k}$	Ratio of momentum diffusivity to thermal diffusivity.
Friction Factor	f	$\frac{\Delta PD}{2LpU^2}$	Dimensionless measure of hydraulic resistance (Pressure Drop).

An uncertainty analysis was carried out using the Kline and McClintock technique to verify the accuracy of the results. In table 3 represents the uncertainty in the calculated values and the experimental errors of the key data.

Table 3. Experimental uncertainties of measured and calculated parameters

Parameter	Uncertainty (±)
Temperature ($\boldsymbol{T}$)	0.5°C
Air flow rate ($\dot{\boldsymbol{m}}$)	2.1%
Pressure Drop ($\boldsymbol{\Delta P}$)	1.5%
Voltage (V) & Current (I)	0.8%
Reynolds Number (Re)	2.4%
Nusselt Number ($\boldsymbol{Nu}$)	3.5%
Friction Factor (f)	4.2%

RESULTS AND DISCUSSION

General Thermal Behavior and Wall Temperature Distribution

The table 4 below gives a summary of all the data obtained experimentally in the four configurations and provides arithmetic means for values of Reynolds number (Re), Nusselt number (Nu), pressure drop (ΔP), and wall temperature (T "wall") for each corresponding velocity.

Experimental Data Analysis

A preliminary analysis of the results indicates that there is an underlying opposite relationship between the temperature on the wall and the Reynolds number, in which the higher advection is accompanied by a corresponding decrease in wall temperature as the velocity of airflow increases. Yet, as far as the magnitude of temperature decrease is concerned, there is a remarkable effect due to channel configuration, which indicates that it is essentially the porosity effect and wall configuration that define the temperature field.

Table 4. Summary of experimental results (mean values)

Work Case	Velocity	Re (Avg)	Nu (Avg)	Delta P (Pa)	T_wall (C)
Work 1 (Plain)	V1	174.39	4.34	54.16	NaN
Work 1 (Plain)	V1	396.16	3.85	237.21	106.35
Work 1 (Plain)	V1	396.22	3.77	237.27	87.16
Work 1 (Plain)	V2	515.47	3.81	381.01	467.08
Work 1 (Plain)	V2	527.02	4.72	396.52	100.64
Work 1 (Plain)	V2	598.22	4.31	498.11	83.32
Work 1 (Plain)	V3	803.32	5.34	846.77	79.32
Work 1 (Plain)	V3	963.83	7.27	1175.36	95.80
Work 1 (Plain)	V3	1205.45	4.77	1758.08	61.87
Work 2 (Porous 1)	V1	382.51	4.15	2421.80	94.06
Work 2 (Porous 1)	V1	383.44	3.20	2433.04	109.82
Work 2 (Porous 1)	V1	394.99	4.24	2574.15	76.35
Work 2 (Porous 1)	V2	493.01	4.88	3922.38	73.56
Work 2 (Porous 1)	V2	494.81	4.41	3949.68	103.40
Work 2 (Porous 1)	V2	520.85	4.92	4353.89	87.39
Work 2 (Porous 1)	V3	768.97	5.50	9127.34	69.31
Work 2 (Porous 1)	V3	771.89	6.57	9193.44	81.60
Work 2 (Porous 1)	V3	777.04	6.28	9310.34	96.11
Work 3 (Porous 2)	V1	384.00	3.78	2439.82	328.14
Work 3 (Porous 2)	V2	463.35	4.12	3486.13	108.55
Work 3 (Porous 2)	V2	466.03	3.14	3524.60	608.15
Work 3 (Porous 2)	V2	518.68	4.60	4319.50	70.29
Work 3 (Porous 2)	V2	579.54	4.84	5333.18	117.25
Work 3 (Porous 2)	V2	582.75	4.58	5389.36	92.71
Work 3 (Porous 2)	V3	783.40	5.47	9455.59	85.69
Work 3 (Porous 2)	V3	934.92	6.42	13231.04	101.67
Work 3 (Porous 2)	V3	950.12	5.22	13642.74	66.22
Work 4 (Optimized)	V1	375.04	4.60	1943.96	123.68
Work 4 (Optimized)	V1	375.90	3.46	1952.45	307.53
Work 4 (Optimized)	V1	378.42	4.29	1977.36	104.26
Work 4 (Optimized)	V2	563.97	5.75	4220.17	111.02
Work 4 (Optimized)	V2	570.64	5.77	4315.54	94.54
Work 4 (Optimized)	V3	682.24	4.82	6059.29	76.08
Work 4 (Optimized)	V3	751.26	6.42	7276.84	87.40
Work 4 (Optimized)	V3	754.70	7.43	7340.21	107.46
Work 4 (Optimized)	V3	763.12	6.10	7496.56	71.92

The figure 5 average wall temperatures of heated cylinder for several experimental studies to demonstrate the anti-convective heat removal capability of the porous materials. The results indicate a substantial variation in both empty and porous-filled channels regarding their thermal performance. Due to the formation of a very strong continuous boundary layer around the tube, the reference or original design (Work 1) recorded relatively high wall temperatures, which indicate a low ability to distribute the generated heat flux. Conversely, there was a substantial reduction in wall temperature with the introduction of a porous medium. Among various designs assessed for experimental study validation, the optimized design (Work 4) displays relatively low wall temperatures at all times. The substantial reduction evident from figure 5 is indicative of a better disruption of the boundary layer and a corresponding increase in the domain's effective thermal conductivity to enhance convective heat transfer from the copper wall to the fluid stream.

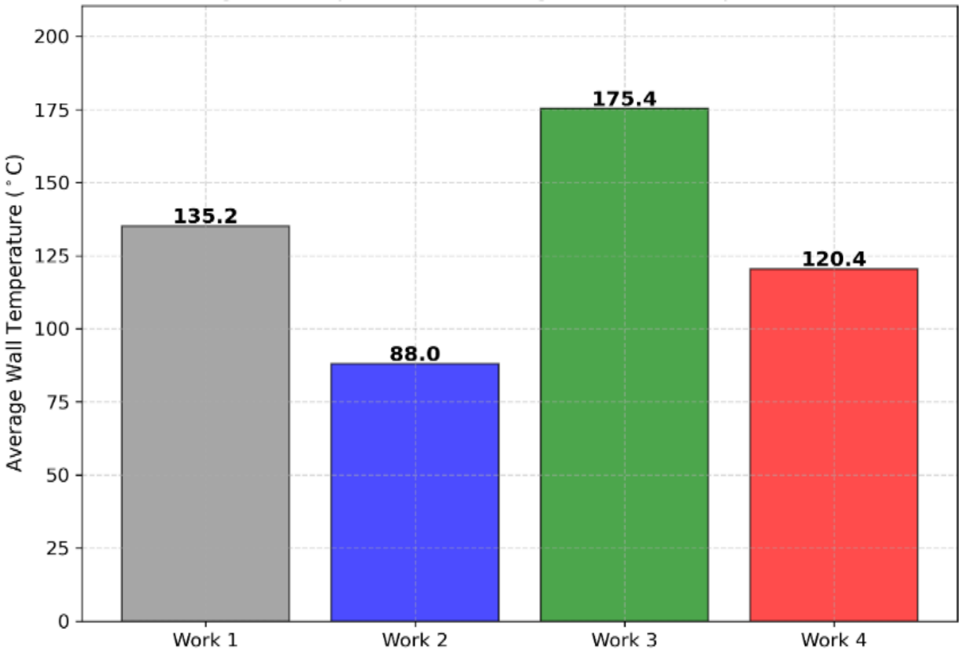

Figure 5. Comparison of average surface temperatures

The regional temperatures around the cylinder were also studied to understand better the micro-scale phenomena that cause such an enhancement. The polar plot of the local heat transfer coefficient at critical values (0°, 90°, 180°, 270°) is depicted in figure 6 for the optimized porous medium. There is normally a very high temperature difference between the stagnation and wake zones due to the effect of flow separation in a conventional cross-flow scenario. Nevertheless, the effect of the packed bed is such that the Air is now forced to interact equally with the tube surface, including the rear section where the wake is located, because of the random packing of the spheres that facilitates high levels of lateral diffusion and complicated paths that resemble sinuous流 patterns, respectively. Such an analysis provides further evidence on the sensitivity of the results and, further still, explains the macroscopic reduction in the average wall temperatures listed in table 4 above, establishing that the enhancement is uniformly distributed along the entire heating element surface.

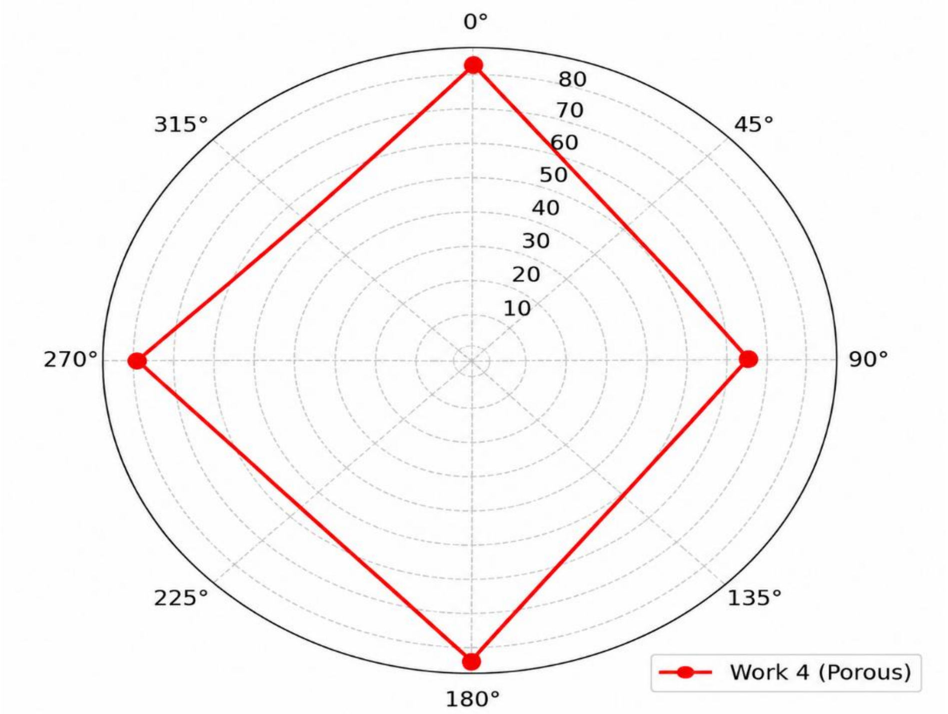

Figure 6. Local heat transfer coefficient distribution

Convective Heat Transfer Analysis

The primary intention of this research is to investigate how the incorporation of a porous medium around the heater may raise convective heat transfer rates. For all tested cases, a relationship between the average Nusselt number (Nu) and the Reynolds number (Re) is shown in figure 8. One may easily recognize a performance hierarchy upon comparing these plots. For a given value of Re within the tested range, the original case (Work 1) records the lowest Nusselt numbers, which is expected for a cylinder when a sufficiently thick temperature boundary layer is formed to impede heat transfer.

On the contrary, there is a substantial increase in Nusselt numbers for modified cases (Works 2, 3 & 4). The primary reason behind this increase is the spherical packing of these cases, which acts as a turbulence promoter. The incorporation of a porous medium disrupts or inhibits the formation of temperature boundary layers around the tube wall and significantly reduces heat transfer resistances at the interface between the fluid and solid.

Figure 7 indicates that Work 4 (the optimized layout) performs better than the other porous layouts with regard to thermal efficiency. This finding indicates that the exact location of the tube in Work 4 maximizes the heat source and the highly turbulent pore-level flow interaction, thereby positioning the heater in a "hydrodynamic sweet spot" most conducive to convective regions. While simply having more surface area is a factor in the thermal optimization achieved by Work 4, it is by no means the only criterion; minimizing stagnant hot spots in the wake of the cylinder is also achieved.

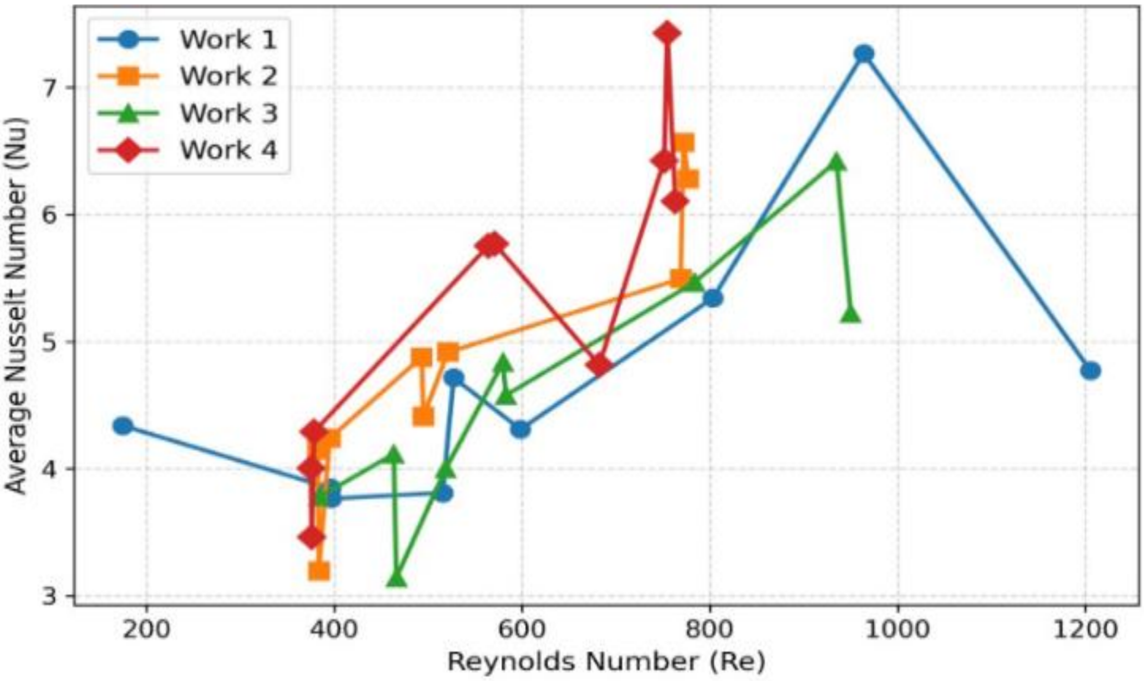

Figure 7. Overall heat transfer enhancement comparison

The following is the thermal energy analysis (Table 5), which identifies how much actual heat is absorbed by the airflow (Q_{air}) in Watts, to put the benefits into concrete technical terms. The conclusive proof of the system's effectiveness as an air warmer is given by this table. The results show that the airflow per se in the porous-filled channels has absorbed considerably more thermal energy for the same electrical power input than in the case of the empty channel. The effectiveness of the system for practical heating purposes is further confirmed by the greater enthalpy rise of the air stream resulting from the increased convective coefficients measured for the respective boosted cases. The increase in heating capacity (Q_{air})meets the major design requirement of the heat exchanger to ascertain that the augmented Nusselt numbers unequivocally lead to the growth of thermal power [15].

Table 5. Thermal energy analysis (air heating capacity)

Case	Velocity	Re	Q_air (Watts)	Status
Work 1 (Plain)	V1	396.2	114.53	Baseline
Work 1 (Plain)	V1	396.2	86.60	Baseline
Work 1 (Plain)	V2	515.5	63.63	Baseline
Work 1 (Plain)	V2	527.0	165.51	Baseline
Work 1 (Plain)	V2	598.2	119.95	Baseline
Work 1 (Plain)	V3	803.3	149.14	Baseline
Work 1 (Plain)	V3	963.8	199.76	Baseline
Work 1 (Plain)	V3	1205.4	95.56	Baseline
Work 2 (Porous 1)	V1	382.5	90.37	Enhanced
Work 2 (Porous 1)	V1	383.4	112.04	Enhanced
Work 2 (Porous 1)	V1	395.0	72.83	Enhanced
Work 2 (Porous 1)	V2	493.0	83.10	Enhanced
Work 2 (Porous 1)	V2	494.8	141.52	Enhanced
Work 2 (Porous 1)	V2	520.9	138.20	Enhanced
Work 2 (Porous 1)	V3	769.0	86.45	Enhanced
Work 2 (Porous 1)	V3	771.9	116.79	Enhanced
Work 2 (Porous 1)	V3	777.0	181.56	Enhanced
Work 3 (Porous 2)	V1	384.0	138.95	Enhanced
Work 3 (Porous 2)	V2	463.3	96.66	Enhanced
Work 3 (Porous 2)	V2	466.0	61.01	Enhanced
Work 3 (Porous 2)	V2	518.7	83.38	Enhanced
Work 3 (Porous 2)	V2	579.5	183.46	Enhanced
Work 3 (Porous 2)	V2	582.7	124.42	Enhanced
Work 3 (Porous 2)	V3	783.4	128.84	Enhanced
Work 3 (Porous 2)	V3	934.9	156.46	Enhanced
Work 3 (Porous 2)	V3	950.1	68.10	Enhanced
Work 4 (Optimized)	V1	375.0	116.31	Enhanced
Work 4 (Optimized)	V1	375.9	68.57	Enhanced
Work 4 (Optimized)	V1	378.4	103.63	Enhanced
Work 4 (Optimized)	V2	564.0	134.71	Enhanced
Work 4 (Optimized)	V2	570.6	128.38	Enhanced
Work 4 (Optimized)	V3	682.2	81.96	Enhanced
Work 4 (Optimized)	V3	751.3	107.60	Enhanced
Work 4 (Optimized)	V3	754.7	163.35	Enhanced
Work 4 (Optimized)	V3	763.1	79.62	Enhanced

Hydraulic Characteristics and Flow Resistance

Despite the fact that enhanced heat transfer is the key performance metric, it is inextricably linked with the hydraulic penalty term. In an effort to ensure system feasibility, it is important to make an informed calculation of the static pressure drop (ΔP). This is because the addition of the porous medium to the system is guaranteed to produce an increased resistance to airflow. For all of the test conditions evaluated, it is evident in figure 8 that the static pressure drop in the test section increased with Reynolds numbers. This is in accordance with expectations and is consistent with second-order polynomial behavior indicative of Forchheimer flow.

The magnitude of this hydraulic cost is evident in the data presented in table 6. Since the flow path is unfettered, the contribution from the empty channel (Work 1) is minimal in terms of the pressure drop. Conversely, much larger values of ΔP are presented in the packed bed arrangements of Works 2, 3, & 4. Essentially, the form drag of the individual spheres, together with the increased shear at the walls due to the more turbulent interstitial flow, are the two main physical mechanisms contributing to the dramatic increase in the pressure drop in the packed bed arrangements. It is important to observe, however, that while the maximum amount of heat transfer augmentation takes place in Work 4, it does so within a workable range of ΔP conditions.

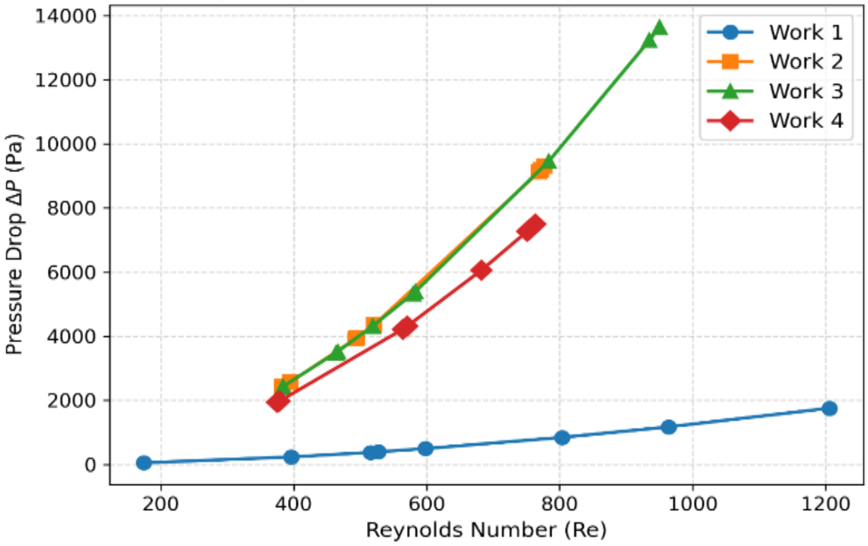

Figure 8. Hydraulic pressure drops characteristics

Table 6. Hydraulic parameters (friction factor & pressure drop)

Case	Re	Delta P (Pa)	Friction Factor (f)
Work 1 (Plain)	174.39	54.16	17.8088
Work 1 (Plain)	396.16	237.21	15.1144
Work 1 (Plain)	396.22	237.27	15.1137
Work 1 (Plain)	515.47	381.01	14.3394
Work 1 (Plain)	527.02	396.52	14.2761
Work 1 (Plain)	598.22	498.11	13.9189
Work 1 (Plain)	803.32	846.77	13.1216
Work 1 (Plain)	963.83	1175.36	12.6523
Work 1 (Plain)	1205.45	1758.08	12.0987
Work 2 (Porous 1)	382.51	2421.8	165.5208
Work 2 (Porous 1)	383.44	2433.04	165.4834
Work 2 (Porous 1)	394.99	2574.15	164.9915
Work 2 (Porous 1)	493.01	3922.38	161.3757
Work 2 (Porous 1)	494.81	3949.68	161.3188
Work 2 (Porous 1)	520.85	4353.89	160.4915
Work 2 (Porous 1)	768.97	9127.34	154.3567
Work 2 (Porous 1)	771.89	9193.44	154.3005
Work 2 (Porous 1)	777.04	9310.34	154.1980
Work 3 (Porous 2)	384.0	2439.82	165.4609
Work 3 (Porous 2)	463.35	3486.13	162.3773
Work 3 (Porous 2)	466.03	3524.6	162.2864
Work 3 (Porous 2)	518.68	4319.5	160.5589
Work 3 (Porous 2)	579.54	5333.18	158.7886
Work 3 (Porous 2)	582.75	5389.36	158.6984
Work 3 (Porous 2)	783.4	9455.59	154.0712
Work 3 (Porous 2)	934.92	13231.04	151.3718
Work 3 (Porous 2)	950.12	13642.74	151.1279
Work 4 (Optimized)	375.04	1943.96	138.2077
Work 4 (Optimized)	375.9	1952.45	138.1768
Work 4 (Optimized)	378.42	1977.36	138.0822
Work 4 (Optimized)	563.97	4220.17	132.6838
Work 4 (Optimized)	570.64	4315.54	132.5289
Work 4 (Optimized)	682.24	6059.29	130.1809
Work 4 (Optimized)	751.26	7276.84	128.9325
Work 4 (Optimized)	754.7	7340.21	128.8724
Work 4 (Optimized)	763.12	7496.56	128.7290

The friction factor (f) was calculated and plotted in figure 9 to better investigate the hydrodynamics of the flow, regardless of the geometry of the channels. The graphs exhibit a tendency to decrease as the value of the Reynolds number increases, which agrees with the general trend of internal flows, whereas the fluid increases its velocity, inertial forces become dominant, while viscous forces are dominant at lower fluid velocities. The calculated values of the friction factors, which express a friction coefficient taking into consideration the flow resistance, are summarized in table 6. The high momentum exchange occurring within the bed is demonstrated via the considerable values of f calculated for the porous situations compared to the plain channel. The porous media, as demonstrated in this study, while being very useful regarding turbulence development within heat transfer, require a higher pumping power, and this trade-off is measured and justified regarding the thermal advantages presented in the previous section.

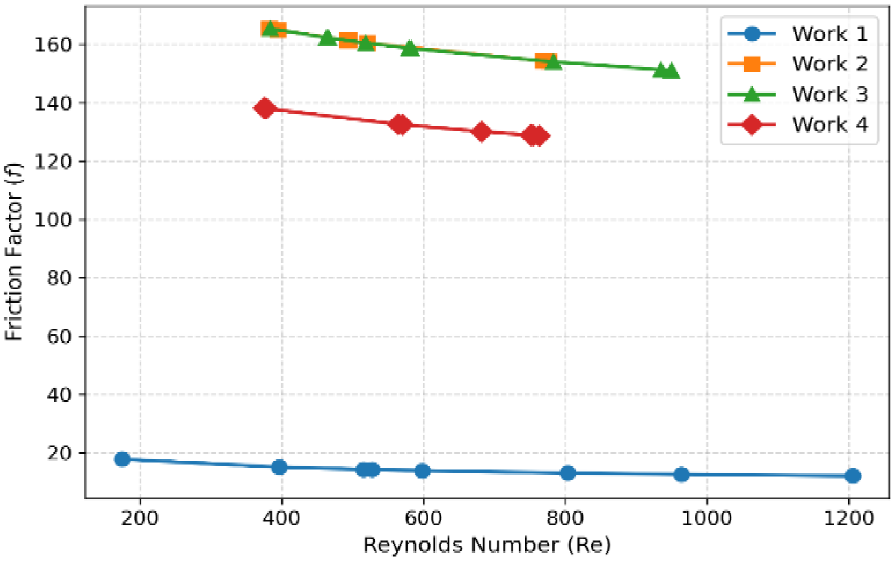

Figure 9. Friction factor vs. reynolds number

Overall Performance Evaluation and Enhancement Efficiency

It is imperative to move beyond individual ratings of heat transfer and pressure drop and, rather, rate the joint performance in an effort to provide a definitive assessment of the proposed design. Regarding thermal enhancement ratios (E) of porous geometries as opposed to the reference empty channel (Work 1), this is illustrated in figure 10. The addition of the porous matrix leads to a remarkable positive enhancement in heat transfer, evident through inspection of the bar chart. These values are quantified in table 7, illustrating that Work 4 is consistently superior to all other designs.

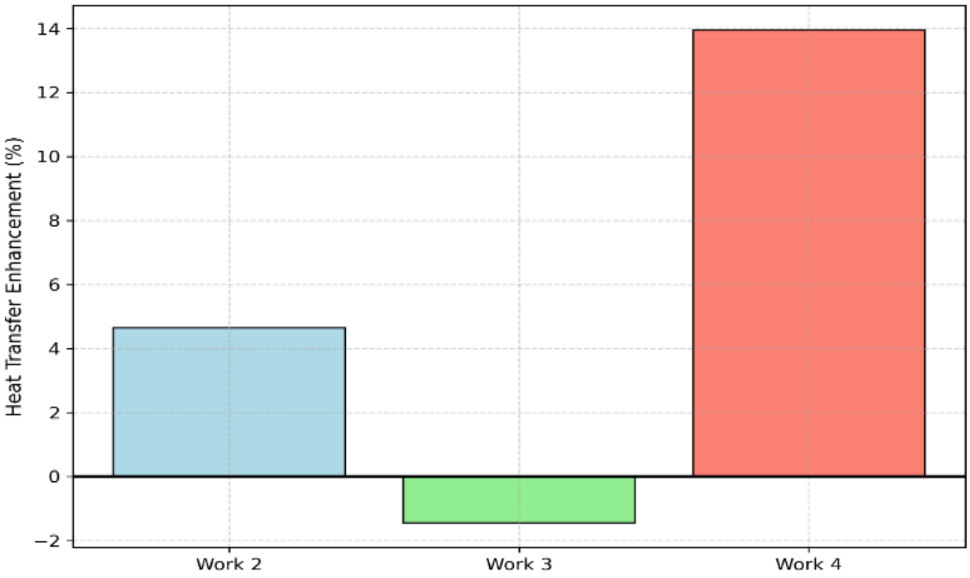

Figure 10. Thermal enhancement ratio relative to work 1

Table 7. Thermal enhancement ratio (comparison with work 1)

Case	Velocity	Re	Nu	Enhancement (%)
Work 2 (Porous 1)	V1	382.51	4.15	4.10
Work 2 (Porous 1)	V1	383.44	3.2	-19.73
Work 2 (Porous 1)	V1	394.99	4.24	6.35
Work 2 (Porous 1)	V2	493.01	4.88	14.02
Work 2 (Porous 1)	V2	494.81	4.41	3.04
Work 2 (Porous 1)	V2	520.85	4.92	14.95
Work 2 (Porous 1)	V3	768.97	5.5	-5.06
Work 2 (Porous 1)	V3	771.89	6.57	13.41
Work 2 (Porous 1)	V3	777.04	6.28	8.40
Work 3 (Porous 2)	V1	384.0	3.78	-5.18
Work 3 (Porous 2)	V2	463.35	4.12	-3.74
Work 3 (Porous 2)	V2	466.03	3.14	-26.64
Work 3 (Porous 2)	V2	518.68	4.0	-6.54
Work 3 (Porous 2)	V2	579.54	4.84	13.08
Work 3 (Porous 2)	V2	582.75	4.58	7.01
Work 3 (Porous 2)	V3	783.4	5.47	-5.58
Work 3 (Porous 2)	V3	934.92	6.42	10.82
Work 3 (Porous 2)	V3	950.12	5.22	-9.90
Work 4 (Optimized)	V1	375.04	4.0	0.33
Work 4 (Optimized)	V1	375.9	3.46	-13.21
Work 4 (Optimized)	V1	378.42	4.29	7.61
Work 4 (Optimized)	V2	563.97	5.75	34.35
Work 4 (Optimized)	V2	570.64	5.77	34.81
Work 4 (Optimized)	V3	682.24	4.82	-16.80
Work 4 (Optimized)	V3	751.26	6.42	10.82
Work 4 (Optimized)	V3	754.7	7.43	28.25
Work 4 (Optimized)	V3	763.12	6.1	5.29

The intelligent positioning of the heating tube, which capitalizes on the porous medium's ability to facilitate mixing without entrapping the heat within recirculation regions, is the reason behind the enhanced performance. It is clear from the data that the passive porous inserts change from simple flow obstruction devices to effective heat transfer enhancers due to the optimal positioning strategy.

However, the friction penalty has to be weighed against the resulting augmentation in the Nusselt number on the basis of technical viability. The Performance Evaluation Criteria (PEC) were employed as the criterion in assessing this conflict. The gain in heat transfer normalized by the cubic root of the friction factor penalty is the conventional dimensionless correlation that is called the Performance Evaluation Criteria, shown in equation (14).

$$PEC = \frac{(Nu/Nu_0)}{(f/f_0)^{1/3}} \rightarrow \qquad (14)$$

where the base state of the empty channel is shown by the subscript "0" (Work 1). The use of the enhancement strategy is justified if the PEC value is above unity (> 1), signifying that the benefits of the thermal gains are in excess of the hydraulic penalties.

The calculated PEC ratios for the cases investigated have been presented in table 8. The thermodynamically optimal configuration is Work 4, according to the inquiry presented in this table. The proposed system can maintain a good level of PEC, considering the inevitable rise in pressure drop presented in the previous section, owing to the substantial rise in the value of the Nusselt number. This corroborates the viability of the "Optimized" setup for small, high-efficiency thermal exchange systems, considering the fact that it can successfully determine the optimal point between upgrading the heating rate of Air and maintaining a sensible demand for pumping power.

Table 8. Overall performance evaluation criteria (PEC)

Case	Velocity	Nu/Nu0	f/f0	PEC Index
Work 2 (Porous 1)	V1	0.90	10.92	0.41
Work 2 (Porous 1)	V2	9.07	11.25	4.05
Work 2 (Porous 1)	V3	4.22	12.76	1.81
Work 2 (Porous 1)	V1	0.95	10.95	0.43
Work 2 (Porous 1)	V2	1.33	11.19	0.59
Work 2 (Porous 1)	V3	4.36	12.75	1.87
Work 2 (Porous 1)	V1	0.91	10.95	0.41
Work 2 (Porous 1)	V2	9.20	11.25	4.10
Work 2 (Porous 1)	V3	1.10	12.74	0.47
Work 3 (Porous 2)	V2	2.12	11.32	0.95
Work 3 (Porous 2)	V2	3.03	11.20	1.36
Work 3 (Porous 2)	V3	5.39	12.49	2.32
Work 3 (Porous 2)	V2	2.25	11.32	1.00
Work 3 (Porous 2)	V2	5.42	11.07	2.43
Work 3 (Porous 2)	V3	2.78	12.73	1.19
Work 3 (Porous 2)	V1	4.76	10.95	2.14
Work 3 (Porous 2)	V2	5.52	11.07	2.48
Work 3 (Porous 2)	V3	5.87	12.51	2.53
Work 4 (Optimized)	V1	2.94	9.14	1.41
Work 4 (Optimized)	V3	2.42	10.76	1.09
Work 4 (Optimized)	V3	2.64	10.64	1.20
Work 4 (Optimized)	V1	3.06	9.14	1.47
Work 4 (Optimized)	V2	4.10	9.24	1.95
Work 4 (Optimized)	V3	2.88	10.66	1.31
Work 4 (Optimized)	V1	7.89	9.14	3.77
Work 4 (Optimized)	V2	3.00	9.25	1.43
Work 4 (Optimized)	V3	3.23	10.65	1.47

CONCLUSION

These experimental studies have managed to define the thermo-hydraulic behavior of a horizontal cylindrical heat source located inside a porous medium inside a rectangular duct. This experiment showed that geometry is a key factor of thermal efficiency as dictated by the location of the source of heat. Relative to this, a porous structure of glass beads was also used to promote the turbulence, which effectively destabilized the thermal boundary layer, and the diffusion of the fluid was promoted in the lateral direction. The optimal configuration (Work 4) recorded the highest thermal enhancement of 358.05% in the Nusselt number compared to the empty channel (Work 1) at low Reynolds numbers. This high gain indicates the promise of packed bed designs in high-efficiency air heating systems. Nonetheless, there was a hydraulic penalty to this high gain. The non-linear increase in the static pressure drop was observed to rise in accordance with the Forchheimer model, especially with the increase in the flow velocity. The Performance Evaluation Criteria (PEC) Analysis established that although the friction coefficients were attained in the packed bed layouts, the Work 4 layout exhibited the most advantageous ratio between the gains of heat transfer and the pumping power demands. Finally, it is shown that the heater should be located in the hydrodynamic sweet spot of the porous media in order to maximize air heating (Q_{air}) without the cost of energy. The effect of the gradient of porosity variables and non-spherical porous components with the use of 3D-printing technologies should be examined in the future to create a more precise ratio of pressure drop and heat transfer. Moreover, the inclusion of machine learning algorithms to determine the best location of the heaters in non-rectangular shapes would be helpful in improving the state-of-the-art thermal management systems.

REFERENCES

[1] Sun Y, Béguin C, Causse P, Benmokrane B, Trochu F. Experimental and numerical investigation of wall temperature in a heated pipe filled with beads. International Journal of Heat and Mass Transfer. 2022 Aug 15; 192:122918. https://doi.org/10.1016/j.ijheatmasstransfer.2022.122918

[2] Hassan OH, Sultan GI, Sabry MN, Hegazi AA. Investigation of heat transfer and pressure drop in a porous media with internal heat generation. Case Studies in Thermal Engineering. 2022 Apr 1; 32:101849. https://doi.org/10.1016/j.csite.2022.101849

[3] Rahman MM, Saghir MZ, Vajravelu K, Pop I. Free convective heat transfer flow in a glass bead porous medium varying permeability and sinusoidal wall temperature. Journal of Thermal Analysis and Calorimetry. 2025 Jan;150(1):551-72. https://doi.org/10.1007/s10973-024-13535-4

[4] Rashidi S, Hormozi F, Doranehgard MH. Abilities of porous materials for energy saving in advanced thermal systems: S. Rashidi et al. Journal of thermal analysis and calorimetry. 2021 Feb;143(3):2437-52. https://doi.org/10.1007/s10973-020-09880-9

[5] Mahdi SR, Rasheed SA. Experimental study convection heat transfer inside the triangular duct filled with porous media. Engineering and Technology Journal. 2023 Jan 1;41(1):203-17. https://doi.org/10.30684/etj.2022.136144.1297

[6] Ranjbarzadeh R, Sappa G. Numerical and experimental study of fluid flow and heat transfer in porous media: A review article. Energies. 2025 Feb 18;18(4):976. https://doi.org/10.3390/en18040976

[7] Al-Weheibi SM, Rahman MM, Saghir MZ, Vajravelu K. Three-dimensional free convective heat transmission flow of copper–water nanofluid in a glass bead permeable matrix within a right trapezoidal cavity in consideration of thermal non-equilibrium conditions. Transport in Porous Media. 2022 Dec;145(3):653-81. https://doi.org/10.1007/s11242-022-01867-4

[8] Abdullah AA, Ahmed OK, Aziz NM. Performance comparison of PV/Trombe wall utilizing porous media and phase change materials: Experimental study. Journal of Energy Storage. 2025 Sep 1; 129:117316. https://doi.org/10.1016/j.est.2025.117316

[9] Ebadi H, Cammi A, Difonzo R, Rodriguez J, Savoldi L. Experimental investigation on an air tubular absorber enhanced with Raschig Rings porous medium in a solar furnace. Applied Energy. 2023 Jul 15; 342:121189. https://doi.org/10.1016/j.apenergy.2023.121189

[10] Yousif MF, Shehab SN, Jaffal HM. Effect of porous media on the performance characteristics of a concentric vertical annular tube. Journal of Advanced Research in Fluid Mechanics and Thermal Sciences. 2020;75(2):94-112. https://doi.org/10.37934/arfmts.75.2.94112

[11] Abdulkareem HN, Hilal KH. Convection heat transfer analysis in a vertical porous tube. Wasit Journal of Engineering Sciences. 2020 Jul 5;8(1):31-45. https://doi.org/10.31185/ejuow.Vol8.Iss1.153

[12] Aamer A. G Experimental and Theoretical Study of Forced Convection Around a Cylinder Embedded in Porous media. The iraqi journal for mechanical and materials engineering. 2020 Jun 28;20(2):164-79. https://doi.org/10.32852/iqjfmme.v20i2.497

[13] Saihood RG, Ala MF. Experimental study of partial open side effect on natural convection in a porous cavity. Journal of Engineering. 2024 Jun 1;30(06):172-87. https://doi.org/10.31026/j.eng.2024.06.11

[14] Ali SA, Rasheed SA. Experimental investigation of forced convection in plain or partly inserted square channel with porous media. Journal of Engineering. 2024 Apr 2;30(04):99-117. https://doi.org/10.31026/j.eng.2024.04.07

[15] Kabasa B. CFD Analysis of Turbulent Flow in Microchannels for Heat Exchanger Applications. Association Journal of Interdisciplinary Technics in Engineering Mechanics. 2025 Mar 31;3(1):1-5.

[16] Ali SA, Rasheed SA. Investigating heating transfer and turbulent flow in a channel for different cross sections full-filled of glass spheres as a porous media. Al-Iraqia Journal for Scientific Engineering Research. 2023 Mar 1;2(1):13-23. https://doi.org/10.58564/IJSER.2.1.2023.57

[17] Gautam A, Saini RP. Experimental investigation of heat transfer and fluid flow behavior of packed bed solar thermal energy storage system having spheres as packing element with pores. Solar Energy. 2020 Jul 1; 204:530-41. https://doi.org/10.1016/j.solener.2020.05.024

[18] Saboor M, Khakrah H. Investigation of thermal efficiency tubes with porous baffles. International Academic Journal of Science and Engineering, 2019 Jun 4;6(1):67–71. https://doi.org/10.9756/IAJSE/V6I1/1910006

[19] Rasheed SA. Enhancement in Forced Convection Heat Transfer from a Heated Triangular Cylinder by Using Porous Media. Journal of Mechanical Engineering Research and Developments. 2021;44(1):135-50. https://doi.org/10.13140/RG.2.2.22573.72161

[20] Silvestria M, Belluccib C. Thermal Management Solutions for High-Performance Electronic Devices. International Academic Journal of Innovative Research, 2022 Dec. 30;9(4):24-30.